

The Anisotropy of Young's Modulus in Bones

Ligia Munteanu¹, Veturia Chiroiu¹ and Valeria Mosnegutu¹

Abstract: In this paper, yet another method for evaluating the elastic modulus for human bones is introduced and investigated. This method adopts the Jankowski and Tsakalakos strain energy function in which, the Born-Mayer energy term is the predominant term for calculations the elastic constants. By taking accounts the directional aspects of the spatial structure of bones, we obtain different values for the Young's modulus depending on the direction of the applied force with respect to the material's structure. The inverse problem analyzed in this paper is solved by inversion of the experimental data. An efficient stopping criterion is adopted to cease the iterative process in order to retrieve stable numerical solutions. The numerical implementation of the aforementioned method is realized by employing a genetic algorithm.

Keywords: Bone, anisotropy, Young's modulus, strain energy function, genetic algorithm.

1 Introduction

Over the last decades, special attention has been given to problems related to the mechanical strength of bones depending on the mass and on the spatial structure of the bones [Allolio (1999); Cummings et al. (1993); Gomberg et al. (2003); Snyder et al. (1993); Veenland et al. (1997); Abdel-Wahab et al (2010)]. The mean intercept length (MIL) and the line frequency deviation (LFD) are two general methods which are used for quantifying directional aspects of the spatial structure of bone. Whitehouse (1974) was the first who describes the anisotropy of bones by means of MIL measurements. For instance, the MIL calculated as a function of the measuring direction yields an ellipse in bone samples [Harrigan and Mann (1984); Cowin (1985); Keaveny et al. (2001)]. The tendency of the MIL to produce nearly perfect ellipses and ellipsoids is due to insensitivity of the MIL to orientation [Geraets (1998); Geraets et al. (2006)]. Sets of densely packed parallel test lines are in principal used to measure MIL and LFD values [Chetverikov (1981); Harrigan and

¹ Institute of Solid Mechanics of Romanian Academy, Bucharest

Mann (1984); Cheal et al. (1987); Turner (1992); Odgaard (1997); Saltikov (1958); Turner (1992)]. Unlike the MIL method, the LFD method can easily be adapted to work with multilevel gray values instead of binary data [Geraets et al. (2006)]. Homminga et al. (2004) investigated the relevance of directional aspects of bone structure with respect to osteoporotic fracture. The trabeculae in osteoporotic vertebrae are oriented predominantly in longitudinal direction, thus providing sufficient stiffness to endure common loading forces but offering less resistance to any load in an off axial direction.

The MIL and LFD methods on one hand and Young's modulus on the other were analyzed by Geraets (1998) and Geraets et al. (2008). These authors have improved the prediction of Young's modulus by combining the LFD with the MIL.

At this stage, it should be mentioned the work of Giesen and Van Eijden (2000) who analyzed the 3D structure of the trabecular bone of the human mandibular condyle. They found that the trabecular structure can withstand larger stresses in parasagittal planes than in the medio-lateral direction, suggesting that the condyle is optimally adapted to sustain stresses and strains occurring *in vivo*. This fact reminds us the Wolff law of bone remodeling [Wolff (1892)], which states that the structure of the bone is optimized to offer maximum resistance to stresses and strains with a minimum amount of mass. An interesting review lecture in this direction has been addressed by Huiskes (2000). It should be noted that Van Ruijven, Giesen and Van Eijden (2002) determined the strains occurring in the mandibular condyle due to static loads, in order to verify that the parasagittal platelike structure of the trabecular bone is optimized to sustain these loads.

As a consequence of the bone anisotropy, the Young's modulus of bones is anisotropic as well [Ashby (1983); Giesen et al. (2001); Van Ruijven et al. (2003)]. It is important to mention that the relationship between the structural and mechanical anisotropy was studied by Van Lenthe and Huiskes (2002).

In general, bones are heterogeneous, inhomogeneous and anisotropic, and for many purposes, they can be treated as linearly elastic solids described by the generalized Hooke's law [Lakes et al. (1975); Lakes and Katz (1979 a,b)]. Depending on the internal symmetry displayed by the bone, the number of elastic constants can be considerably reduced. Because of the symmetry, 21 constants are sufficient to describe the complete mechanical behavior. Estimation of the elastic constants depends on the strain energy function. Consequently, special care should be taken when choosing the form of the strain energy function associated with the human condyle bones.

Motivated by this fact and encouraged by the recent results of Geraets *et al.* (2008), we decided to present in this paper yet another method for evaluating the elas-

tic modulus for human bones, in particular for trabecular bone of the mandibular condyle. This method adopts the Jankowski and Tsakalakos energy strain function [Jankowski and Tsakalakos (1985); Jankowski (1988)] in which, the Born-Mayer elastic term is the predominant term for calculations the elastic constants

$$E_r = \frac{1}{2} \alpha \sum_R \exp(-\beta R), \quad (1)$$

where α and β are unknown parameters depending of the mandibular condyle mechanical behavior. The sum is extended to all the nearest neighbors who are located at distances $R^{(n)}$. For a cell volume Ω containing the bone sample, the second-order elastic constants (stiffness constants) C_{ijkl} , $i, j, k, l = 1, 2, 3$, are evaluated as

$$C_{ijkl} = \frac{1}{\Omega} \frac{\partial^2 E_r}{\partial \varepsilon_{ij} \partial \varepsilon_{kl}}, \quad i, j, k, l = 1, 2, 3. \quad (2)$$

The main advantage of the Jankowski and Tsakalakos energy strain function is that of simplicity and convergency when coupled to the experimental data in order to find the unknown parameters, a very desirable feature from the computational point of view. Consequently, the inversion of the experimental data has a stable character when accompanied by a suitable stopping criterion. Unknown parameters may result in a reduced number of iterations performed by the genetic algorithm and hence reduced computational time.

The paper is organized as follows: Sect.2 is devoted to the calculation of the Young's modulus for an anisotropic body subject to arbitrary small initial deformations, by using the Jankowski and Tsakalakos energy strain function. The inverse problem for the evaluation of the unknown parameters is presented in Sect. 3. Next section presents the results of the method regarding the evaluation of the Young's modulus for the human condyle bones. Finally, concluding remarks are provided in Sect.5.

2 The Calculation of the Young's Modulus

Let us consider a cell volume Ω of the bone sample, embedded into a 3D box of dimensions $a \times b \times c$ mm³. A number N of elementary cells with the elementary cell size of $a_v \times b_v \times c_v$ μ m³ divide the box. The trabecular bone is modeled as a periodic structure with three different materials [Singh (1978)], namely the types A, B and C, respectively. Type A is formed of fine straight or curved rods 0.08-0.14mm in diameter and about 1mm in length. Type B is made up of plates arranged parallel to each other and connected by numerous rods. The plates are 0.16-0.3mm thick, a few millimeters long and are separated by a gap of 0.4-0.8mm. Type C is constituted of irregular plates of 0.12-0.24mm thick with numerous fenestrations.

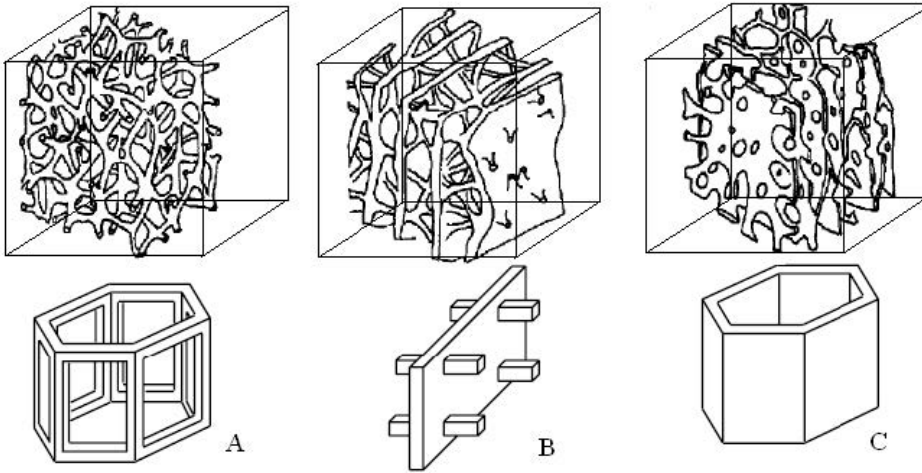


Figure 1: Three types of trabecular bone (after Singh (1978)) and corresponding elementary cells (after Zysset (1994)).

The plates enclose tubular spaces of 0.7-2mm in diameter. Figure 1 represents the types of trabecular bone and also, the elementary cells of the periodic model for the trabecular bone, respectively [Zysset (1994)]. In this Section we admit that the bone sample has known shape and volume.

We adopt the Jankowski and Tsakalagos model (1.1) in which, the Born-Mayer repulsive energy term is the predominant term for calculations the elastic constants. The second-order elastic constants (stiffness constants) are determined by Eq. (1.2). To derive the general formulae for the Young's modulus in the case of an anisotropic body subject to arbitrary small initial deformations, we start with the previously results of Delsanto, Provenzano and Uberall (1992) regarding the differentiation with respect to ε_{ij} of a given function

$$\frac{\partial}{\partial \varepsilon_{ij}} = \frac{1}{2} \left(X_i \frac{\partial}{\partial x_j} + X_j \frac{\partial}{\partial x_i} \right). \quad (3)$$

In Eq. (2.1) X_i are the Lagrangian coordinates corresponding to an initial state which may be subject to an initial finite deformation, x_i are the final Eulerian coordinates, differing from X_i by an infinitesimal deformation. Using Eq. (2.1) it is straightforward to prove that, for a differentiable function $f(r)$, the following relation holds

$$\left(\frac{\partial^2 f(r)}{\partial \varepsilon_{kl} \partial \varepsilon_{ij}} \right)_{r=R} = \frac{1}{R^3} [Rf''(R) - f'(R)] Y_{ijkl} + \frac{1}{4R} f'(R) Z_{ijkl}, \quad (4)$$

where

$$Y_{ijkl} = X_i X_j X_k X_l, \quad (5)$$

$$Z_{ijkl} = X_i X_k \delta_{jl} + X_i X_l \delta_{jk} + X_j X_l \delta_{ik} + X_j X_k \delta_{il}, \quad (6)$$

$$R = \sqrt{X_1^2 + X_2^2 + X_3^2}. \quad (7)$$

Applying Eqs. (2.2)-(2.5) to Eqs. (1.4) and (1.5), it follows that

$$C_{ijkl} = \frac{1}{\Omega} \frac{\partial^2 E_r}{\partial \varepsilon_{ij} \partial \varepsilon_{kl}} = A_{ijkl} - B_{ijkl}, \quad (8)$$

where

$$A_{ijkl} = \sum_n f^{(n)} Y_{ijkl}^{(n)}, \quad (9)$$

$$B_{ijkl} = \sum_n g^{(n)} Z_{ijkl}^{(n)}, \quad (10)$$

$$f^{(n)} = f(R^{(n)}) = 4g^{(n)} \left[1 + \frac{\beta R^{(n)}}{(R^{(n)})^2} \right], \quad (11)$$

$$g^{(n)} = g(R^{(n)}) = \frac{K}{R^{(n)}} \exp(-\beta R^{(n)}), \quad (12)$$

where K is defined as

$$K = \frac{\alpha \beta}{8\Omega}, \quad (13)$$

and $Y^{(n)}$, $Z^{(n)}$ and $R^{(n)}$ refer to the corresponding quantities defined in Eqs. (2.3), (2.4) and (2.5) respectively, as calculated for the n -th nearest neighbor.

In order to simplify the calculation of the elastic constants, it is useful to observe that the number of terms to be evaluated explicitly may be greater reduced due to some special symmetries, in addition to the usual symmetries of C_{ijkl} .

We use here Voigt's convention to denote each pair of indices of the elastic constants by a single index $(i, j) \rightarrow i\delta_{ij} + (9 - i - j)(1 - \delta_{ij})$. According to this convention we have $C_{klmn} = C_{\alpha\beta}$, where the Latin subscripts range over the values 1,2,3, while the Greek subscripts range over the values 1,2,...,6. Therefore, 6 independent elastic constants can be calculated next

$$C_{11} = C_{22} = A_{11} - B_{11}, \quad C_{12} = A_{12} - B_{12}, \quad C_{13} = C_{23} = A_{13} - B_{13},$$

$$\begin{aligned}
 C_{14} = -C_{24} = C_{56} = A_{14} - B_{14}, \quad C_{33} = A_{33} - B_{33}, \\
 C_{44} = C_{55} = A_{44} - B_{44}, \quad C_{66} = (C_{11} - C_{12})/2,
 \end{aligned} \tag{14}$$

for the structures A and C, and 9 independent elastic constants

$$\begin{aligned}
 C_{11} = A_{11} - B_{11}, \quad C_{12} = A_{12} - B_{12}, \quad C_{13} = A_{13} - B_{13}, \\
 C_{22} = A_{22} - B_{22}, \quad C_{23} = A_{23} - B_{23}, \quad C_{33} = A_{33} - B_{33}, \\
 C_{44} = A_{44} - B_{44}, \quad C_{55} = A_{55} - B_{55}, \quad C_{66} = A_{66} - B_{66},
 \end{aligned} \tag{15}$$

for the structure B, where

$$\begin{aligned}
 A_{11} = \frac{2}{3}f_c\eta'^4, \quad A_{12} = \frac{1}{6}(f_a + f_c)\eta^2, \quad A_{13} = \frac{1}{6}f_c\eta^2\eta'^2, \quad A_{14} = \frac{1}{12\sqrt{2}}f_c\eta^3\eta', \\
 A_{22} = \frac{1}{16}(9f_a + f_c)\eta^4, \quad A_{23} = \frac{1}{16}(9f_a + f_c)\eta^2\eta'^2, \quad A_{33} = \frac{1}{16}(9f_a + f_c)\eta^4, \\
 A_{44} = \frac{1}{8}(9f_a + f_c)\eta^2\eta'^2, \quad A_{55} = \frac{1}{8}(f_a + 9f_c)\eta^4, \quad A_{66} = \frac{1}{16}(f_a + 3f_c)\eta'^4,
 \end{aligned}$$

$$\begin{aligned}
 B_{11} = 8g_c\eta'^2, \quad B_{12} = (g_a + 6g_c)\eta'^2, \quad B_{13} = \frac{1}{6}(2g_a + 3g_c)\eta'^2, \\
 B_{14} = \frac{1}{16}(g_a + 3g_c)\eta\eta', \quad B_{22} = (6g_a + 2g_c)\eta'^2, \quad B_{23} = \frac{1}{2}[3g_a\eta'^2 + 4g_c\eta'^2], \\
 B_{33} = \frac{2}{3}[3g_a\eta'^2 + g_c\eta'^2], \quad B_{44} = \frac{2}{3}[3g_a\eta'^2 + g_c\eta'^2], \\
 B_{55} = \frac{1}{2}[3g_a\eta'^2 + g_c(\eta'^2 + 4\eta'^2)], \quad B_{66} = \frac{1}{6}[g_c(\eta'^2 + 4\eta'^2)],
 \end{aligned}$$

$$f_a = f(R_a), \quad f_c = f(R_c), \quad g_a = g(R_a), \quad g_c = g(R_c),$$

$$R_a = \frac{1}{\sqrt{2}}\eta a, \quad R_c = a\sqrt{\frac{1}{3}\eta'^2 + \frac{1}{6}\eta^2}, \quad \eta = 1 + \varepsilon, \quad \eta' = 1 + \varepsilon'.$$

The functions f and g are explicitly defined by Eqs. (2.9) and (2.10). A comparison of the proposed method of calculation the Young's modulus with the classical methods was previously analyzed by Delsanto, Provenzano and Uberall (1992). The conclusion is that the proposed theory allows an easy identification of only two parameters by using a genetic algorithm based on the inversion of the experimental data [Chiroiu, Munteanu and Toader (2010)].

3 The Inverse Problem

In order to evaluate the Jankowski and Tsakalakos strain energy function (1.1), the unknown parameters α and β have to be extracted from the experimental data. For this purpose, we develop the problem based on the relationship between the form and the function in bones, produced and maintained by mechanical forces.

Consider that the human mandibular condyle specimen is embedded into a 3D box of dimensions $a \times b \times c \text{ mm}^3$ and divided into N elementary cells of size $a_v \times b_v \times c_v \mu\text{m}^3$. This cell volume was analyzed by Giesen and Van Eijden (2000) and Van Eijden et al. (2006).

The underformed condyle specimen in the stress-free reference state, and possible deformation of the condyle in the midsagittal cross-section are shown in Figure 2. In all simulations, the condyle is subjected to uniaxial load (tension and compression) and torsion (shear) respectively. The gray colour indicates the unloaded shape, and the deformed shapes are depicted by lines. At the bottom, the deformation is zero, because the saw plane is fixed during the simulation. Let us suppose that the underformed specimen surface is modeled as an ellipsoid surface S defined by the implicit equation [Bardinet, Cohen and Ayache (1994); Munteanu, Chiroiu and Chiroiu (2002)]

$$S \equiv \left[\left(\frac{X_1}{a_1} \right)^{\frac{2}{c_2}} + \left(\frac{X_2}{a_2} \right)^{\frac{2}{c_2}} \right]^{\frac{c_2}{c_1}} + \left(\frac{X_3}{a_3} \right)^{\frac{2}{c_1}} - 1 = 0, \tag{16}$$

where the constants $a_i, i = 1, 2, 3$ and $c_i, i = 1, 2$, are unknown. For a sphere of radius R we have $c_1 = c_2 = 1$ and $a_1 = a_2 = a_3 = R$, respectively. The X_3 -axis corresponds to the X_3 -axis of inertia of the ellipsoid model.

For determining of the unknown constants $z_j = \{a_1, a_2, a_3, c_1, c_2, \alpha, \beta\}, j = 1, \dots, 7$, we formulate an inverse problem closely related to the Wolff law which states that the structure of bone is optimized to offer maximum resistance to stresses and strains with a minimum amount of bone mass [Popescu and Chiroiu (1981)]. The inverse problem combines the minimum volume and the minimum compliance problems, respectively:

Inverse problem: Determine the Jankowski and Tsakalakos energy strain function (1.1) and the unknown surface S of the condyle specimen defined by Eq. (3.1) from

$$\begin{aligned} & \text{minimize}_{z_j, u} \int_{\Omega} \gamma(x_1, x_2, x_3) dx_1 dx_2 dx_3, \text{ and} \\ & \text{minimize}_{z_j, u} f^T u, \\ & \text{subject to } K(z_j)u = f, \end{aligned} \tag{17}$$

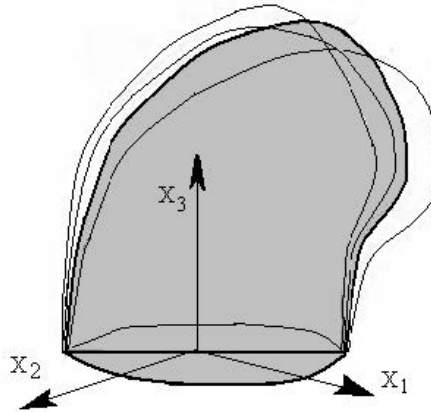


Figure 2: Possible deformations of the mid-sagittal cross-section of the condyle specimen (after Van Ruijven et al. (2002)).

where x_i are the Eulerian coordinates, γ is a function which depends on the unknown surface S defined by Eq. (3.1), $K(z_j)$ is the stiffness matrix, f is the vector of the static external loads and u is the corresponding displacement vector determined by the equilibrium equations $K(z_j)u = f$.

The static loading cases include the uniaxial test (tension and compression) and the torsion test (shear). The loading vector f is determined from the strain field inside the trabecular bone due to static loading evaluated by Van Ruijven, Giesen and Van Eijden, (2002) and additional experimental data [Hou et al. (1998); Kabel et al. (1999)].

Van Ruijven, Giesen and Van Eijden, (2002) calculated the supero-inferior, the medio-lateral and the antero-posterior μ -strain for all loadings (anterior load, apical load and posterior load). The maximum values of the μ -strains are -3301 ± 1720 for the posterior load (supero-inferior) and 2762 ± 1241 for posterior load (antero-posterior). The minimum values are -26 ± 186 for the apical load (medio-lateral) and 54 ± 210 for anterior-load (medio-lateral). Consequently, the range of f is estimated to be between 40N and 145N.

The inverse problem (3.2) is solved by using a genetic algorithm. We use a binary vector with 7 genes representing the real values of the parameters z_j , $j = 1, 2, \dots, 7$. The length of the vector depends on the required precision, which in this case are six places after the decimal point. The domain $z_j \in [-a_j, a_j]$ with length $2a_j$ is divided into a least 15000 equal size ranges. That means that each parameter z_j , $j = 1, 2, \dots, 7$, is represented by a gene (string) of 22 bits ($2^{21} < 3000000 \leq 2^{22}$). The

alternation of generations is stopped when convergence is detected. The stopping criteria are defined with a function that receives the actual state of the genetic algorithm: the actual solution, the actual (maximal) fitness, the actual population with all the fitness. This function returns a boolean that says if the execution must be interrupted or not.

4 Results

As has been stated before, a genetic algorithm was used to solve the inverse problem (3.2). The genetic algorithm was carried out for the number of populations 20, ratio of reproduction 1.0, number of multi-point crossovers 1, probability of mutation 0.2 and maximum number of generations 200. We have considered a bone sample embedded into a 3D box of dimensions $a = 3.5\text{mm}$, $b = 3.5\text{mm}$ and $c = 3.4\text{mm}$. This volume is divided into N elementary cells of size $34 \times 34 \times 34 \mu\text{m}^3$. The density of bone is defined as the weight of the bone phase divided by the total volume ($\rho = 0.160\text{-}0.950 \text{ g/cm}^3$).

We report in this section the results of the genetic algorithm obtained after 234 iterations for $N = 40.833(3) \times 10^7$. The quality of solutions is measured by the accuracy errors ε_V for the volume, and ε_A for the surface S area, respectively

$$\varepsilon_V = \frac{V(S_N)}{V(S)} - 1, \quad \varepsilon_A = \frac{A(S_N)}{A(S)} - 1, \quad (18)$$

where N is the number of the elementary cells. Figure 3 presents the accuracy errors as functions of the number of elementary cells. From the figure it can be seen that as N increases then ε_V and ε_A decrease. Therefore, the inverse problem admits a convergent and stable numerical solution for $N \geq 40.833(3) \times 10^7$.

Once the convergence with respect to N has been established, a noisy version of the loading vector f can be written by multiplication it by $1 + r$, r being random numbers uniformly distributed in $[-\varepsilon, \varepsilon]$, with $\varepsilon = 10^{-1}$, $\varepsilon = 10^{-2}$ and $\varepsilon = 10^{-3}$, respectively. Figure 4 presents the accuracy error ε_A , as functions of the level of noise added into the loading vector. From the figure it can be seen that the iterative process is convergent with respect to increasing the number of iterations for $\varepsilon = 10^{-2}$ and $\varepsilon = 10^{-3}$. In this case, the accuracy errors keep decreasing even after a large number of iterations. The situation is different for $\varepsilon = 10^{-1}$. The accuracy errors decrease up to a certain iteration number and after that they start increasing. If the algorithm is continued beyond this point then the numerical solutions lose their smoothness and become unstable, i.e. highly oscillatory and unbounded. Therefore, a stopping criterion must be introduced in order to finish the iterative process at the point where the errors in the numerical solutions start increasing.

We specify that the accuracy error exhibits a similar behavior.

The first result of the genetic algorithm consists in the estimation of the constants required by the condyle specimen surface S given by Eq. (3.1)

$$c_1 = c_2 = 0.245, \quad a_1 = a_2 = 0.722R, \quad a_3 = R, \quad (19)$$

with $R = 0.0619\text{m}$ for the particular bone considered in this paper. Next, the constants α (units Ryd (Rydberg) $1 \text{ Ryd} = 13.6 \text{ eV} = 2.092 \times 10^{-21} \text{ J}$) and β (units ua in units of a^{-1} where a is the elementary cell lattice constant) are shown in Table 1. The constants have different values depending of the type of loading. It is important to say that α affects only the absolute values of the elastic constants and moduli as a multiplicative constant. Once the constants α and β are known for each type of trabecular bone, the strain energy function (1.4) can be evaluated.

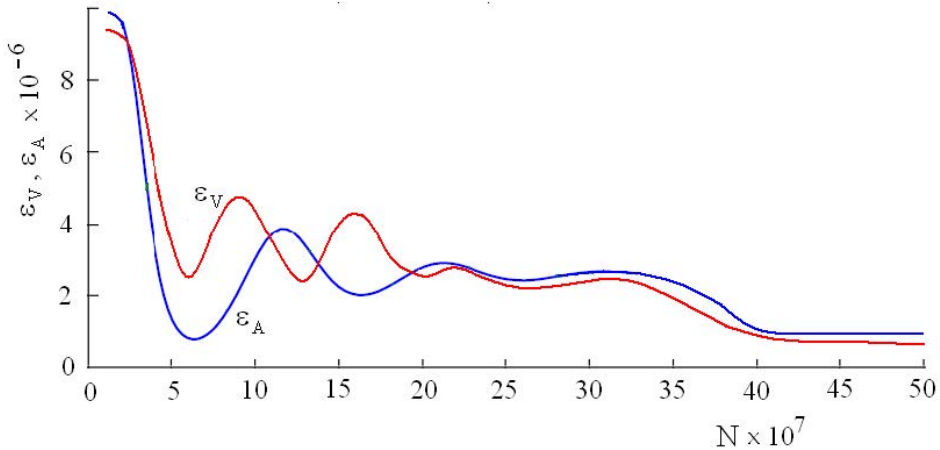


Figure 3: Relative errors $\varepsilon_V, \varepsilon_A$ as functions of N .

Elastic constants evaluated for each type of bone are listed in Table 2. It should be mentioned that the comparison of our results with similar data by others is not available, but we believe that it is useful to mention here some results obtained by mechanical testing methods or ultrasonic wave propagation techniques by several investigators for various bones. For instance, Lang (1969, 1970) found $C_{11} = 19.7 \text{ GPa}$, $C_{12} = 12.10 \text{ GPa}$, $C_{13} = 12.6 \text{ GPa}$, $C_{33} = 32.00 \text{ GPa}$, $C_{44} = 5.40 \text{ GPa}$, $C_{66} = 3.80 \text{ GPa}$ for bovine phalanx. For the bovine femur dried, the aforementioned authors obtained $C_{11} = 23.80 \text{ GPa}$, $C_{12} = 10.20 \text{ GPa}$, $C_{13} = 11.20 \text{ GPa}$, $C_{33} = 33.40 \text{ GPa}$, $C_{44} = 8.20 \text{ GPa}$, $C_{66} = 10.20 \text{ GPa}$. For the bovine femur, Van Buskirk et al (1981) obtained $C_{11} = 16.25 \text{ GPa}$, $C_{12} = 6.34 \text{ GPa}$, $C_{13} = 5.89 \text{ GPa}$, $C_{33} = 25.00 \text{ GPa}$, $C_{44} = 6.65 \text{ GPa}$, $C_{66} = 4.96 \text{ GPa}$.

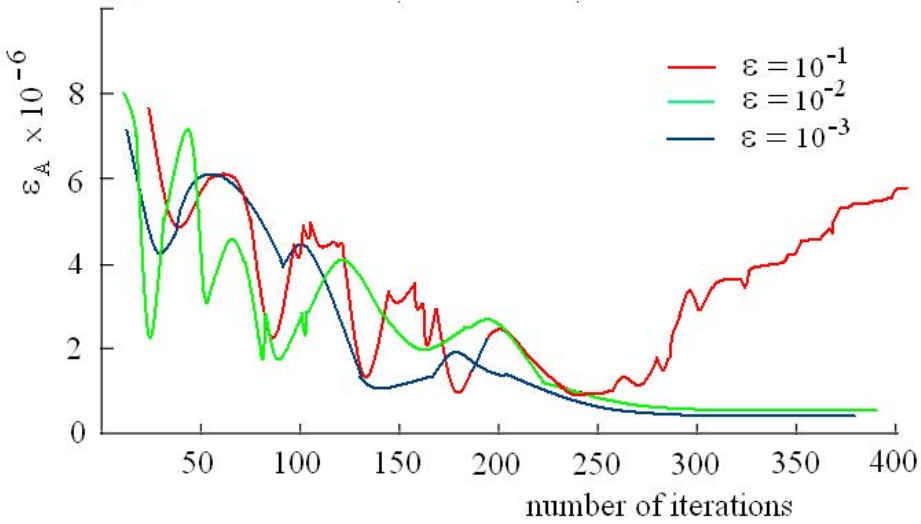


Figure 4: Relative error ϵ_A for three levels of noise added into the loading vector.

Table 1: Energy constants for each type of bone.

Constants	A	B	C
α	0.23 tension	0.25 tension	0.21 tension
	0.32 compression	0.34 compression	0.30 compression
	0.41 shear	0.42 shear	0.39 shear
β	0.50 tension	0.52 tension	0.44 tension
	0.76 compression	0.83 compression	0.71 compression
	0.29 shear	0.35 shear	0.26 shear

We have to also mention that the constant C_{44} may exhibit negative values for large positive deformations, as shown in Figure 5. The constant C_{44} represents resistance to shear. For most materials, the shear modulus is two times to three times greater than Young's modulus, but it is possible (for prestrained materials) to obtain a negative shear modulus. Estimated results for the Young's modulus profile are shown for each type of bone in Figures 6, 7 and 8, respectively. Right sides illustrate the computed LFD profiles. For measuring the LFD profiles, first the fraction of pores is calculated for each test line separately and then the standard deviation of these fractions yields [Geraets et al. (1997); Geraets et al. (1998); Geraets (1998)]. Close examination of the Young's modulus profiles reveals a good similarity of the type C of bone with the shape corresponding to one of the structures generated

by Van Lenthe and Huiskes (2002), Geraets (1998) and Geraets et al. (2008), respectively. For the types A and B, respectively, we obtained different profiles on Young's modulus in comparison to the results of aforementioned authors.

Figure 9 provides the stress-strain constitutive law in the axial (coronal) and transverse (sagittal) directions for the type A of bone.

Table 2: Elastic constants for each type of bone.

Constants [GPa]	A	B	C
C_{11}	20.44	21.23	18.45
C_{12}	13.28	14.77	12.98
C_{13}	13.28	13.97	11.98
C_{14}	9.55	0	9.34
C_{22}	20.44	24.44	18.45
C_{23}	13.28	11.05	11.98
C_{24}	-9.55	0	-9.34
C_{33}	23.20	24.44	22.89
C_{44}	11.30	11.69	11.26
C_{56}	9.55	0	9.34
C_{55}	11.30	11.62	11.26
C_{66}	3.58	3.95	2.74

5 Conclusions

A good evaluation of the mechanical anisotropy is the mean intercept length (MIL). By measuring the distance between two successive bone-marrow transitions for a number of spatial orientations, an ellipsoid can be fitted through the data points. But the ellipsoids are not always sufficient to describe the anisotropy of the Young's modulus or other mechanical properties of bones [Gomberg et al. (2003); Hoffmeister et al. (2000); Pidaparti and Turner (1997)]. By analyzing the spatial structures of bone, Geraets et al (2008) have adopted an interesting method to use the MIL and the line frequency deviation (LFD) combined. Unlike the MIL method the LFD method can easily be adapted to work with multilevel gray values instead of binary data [Geraets et al. (2006)].

In this paper, yet another method for evaluation of the Young's modulus of human mandibular condyle bones was proposed, based on the Jankowski and Tsakalagos strain energy function. The elastic constants are computed by using the classical definition and the previously results by Delsanto, Provenzano and Uberall (1992) regarding the differentiation of a function with respect to deformations. The strain

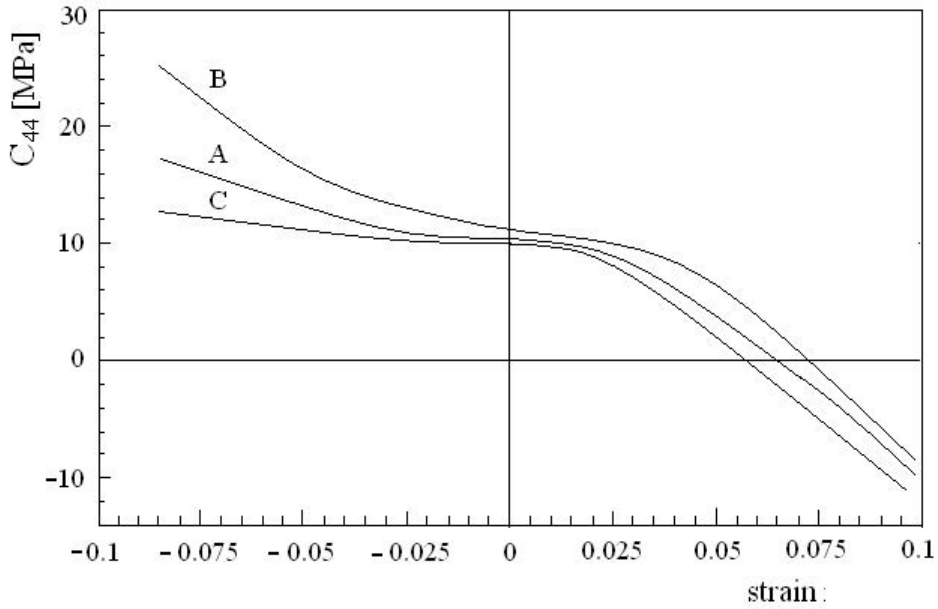


Figure 5: Plot of elastic constant C_{44} versus deformation.

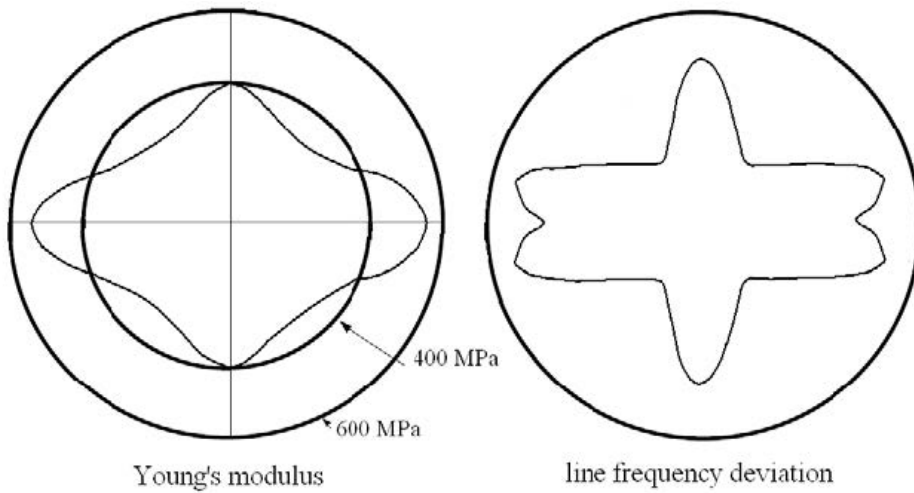


Figure 6: Estimated Young's modulus profile for the type A of bone.

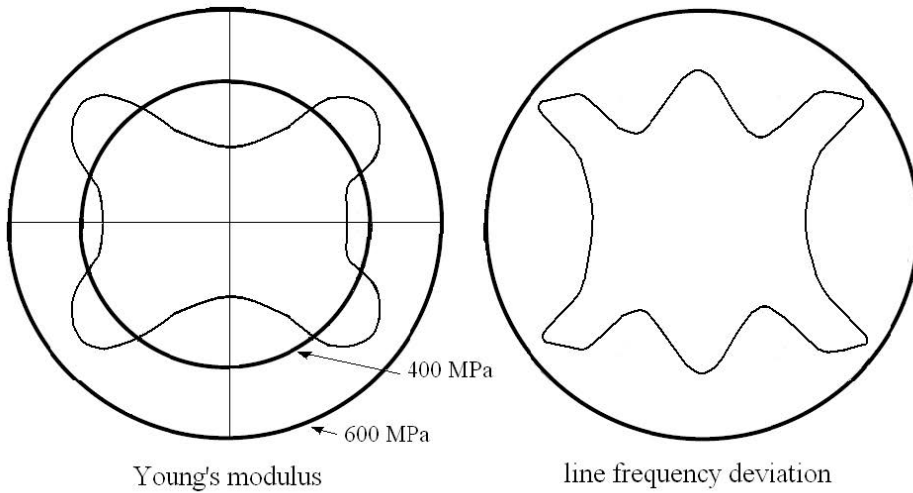


Figure 7: Estimated Young's modulus profile for the type B of bone.

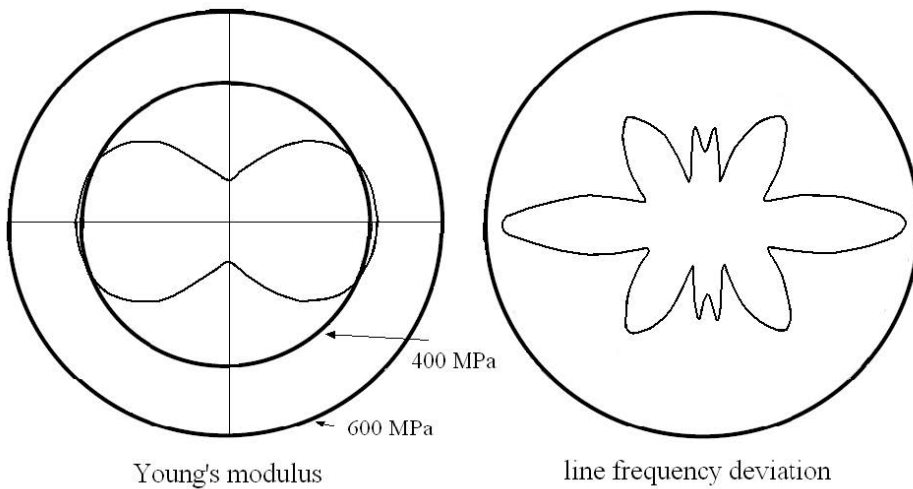


Figure 8: Estimated Young's modulus profile for the type C of bone.

energy function requires the choice of two constants, whilst the underformed bone surface modeled as an ellipsoid surface, requires the choice of five constants. The estimation of these constants is achieved by using an inverse problem which combines the minimum volume problem and the minimum compliance problem.

The numerical results obtained by using a genetic algorithm showed that the in-

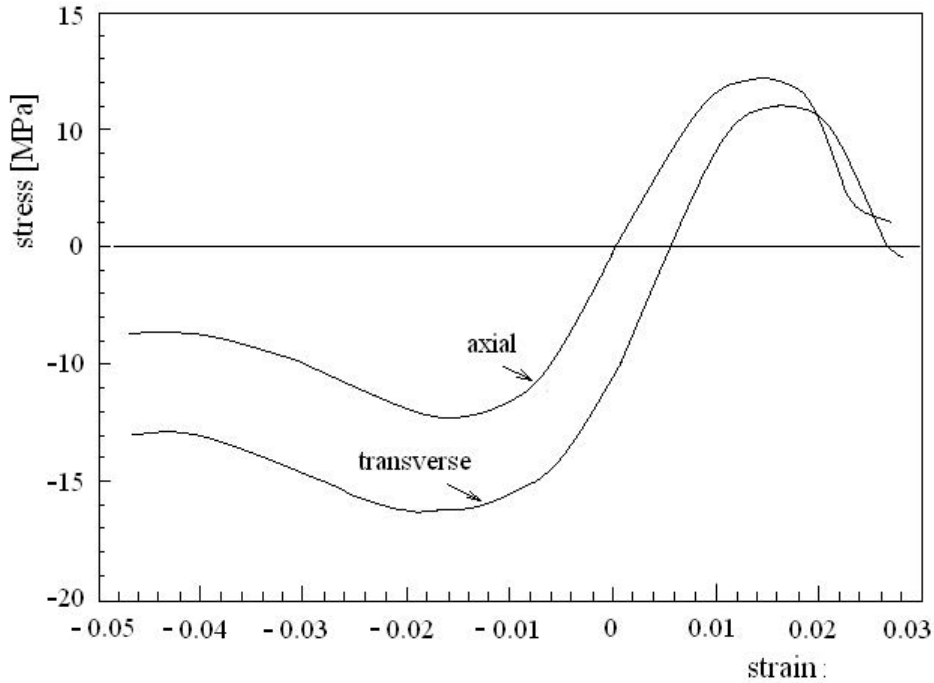


Figure 9: Constitutive law in the axial and transverse directions for the type A of bone.

verse problem produces a convergent and stable numerical solution with respect to increasing the number of the elementary cells and decreasing the amount of noise, respectively. Furthermore, the proposed method was also compared with MIL and LFD. It was shown that, in terms of accuracy, our method completes with new information the results of aforementioned methods.

Future work will be related to the mineralization effect on the stress and strain distribution in the mandibular condylar bone.

References

Abdel-Wahab, A.A.; Maligno, A.; Silberschmidt, V.V. (2010): Dynamic properties of cortical bone tissue: Izod tests and numerical study. *CMC: Computers, Materials & Continua* 19(3): 217–238.

Allolio, B. (1999): Risk factors for hip fracture not related to bone mass and their therapeutic implications. *Osteoporosis International Suppl. 2*: s9–s16.

- Ashby, M.F.** (1983): The mechanical properties of cellular solids. *Metallurgical Transactions* 14A: 1755–1769.
- Bardinet E.; Cohen L.; Ayache, N.** (1994): Fitting of iso-surfaces using superquadrics and free-form deformations. In Proceedings IEEE Workshop on Biomedical Image Analysis (WBIA), Seattle, Washington.
- Cheal, E.J.; Snyder, B.D.; Nunamaker, D.M.; Hayes, W.C.** (1987): Trabecular bone remodeling around smooth and porous implants in an equine patellar model. *Journal of Biomechanics* 20: 1121–1134.
- Chetverikov, D.** (1981): Textural anisotropy features for texture analysis. In: Proceedings of the 5th IEEE Computer Society Conference on Pattern Recognition and Image Processing, Dallas 583–588.
- Chiroiu, V.; Delsanto, P.P.; Munteanu, L.; Rugin?, C.; Scalerandi, M.** (1987): Determination of the second-and third-order elastic constants in Al from the natural frequencies, *Journal of the Acoustical Society of America* 102(1).
- Chiroiu, C.; Munteanu, L.; Chiroiu, V.; Delsanto, P.P.; Scalerandi, M.** (2000): A genetic algorithm for determining of the elastic constants of a monoclinic crystal. *Inverse Problems, Institute of Physics Publishing* 16:121–132.
- Chiroiu, V.; Munteanu, L.; Toader, A.** (2010): Optimum design of a thin elastic rod using a genetic algorithm. *CMES: Computer Modeling in Engineering & Sciences*, 65(1): 1–26.
- Cummings, S.R., Black, D.M., Nevitt, M.C., Browner, W., Cauley, J., Ensrud, K.** (1993): Bone density at various sites for prediction of hip fractures. *Lancet* 341, 72–75.
- Cowin, S.C.** (1985): The relationship between the elasticity tensor and the fabric tensor. *Mechanics of Materials* 4: 137–147.
- Delsanto, P.P.; Provenzano, V.; Uberall, H.** (1992): Coherency strain effects in metallic bilayers. *J. Phys., Condens. Matter.* 4: 3915–3928.
- Donescu, St.; Chiroiu, V.; Munteanu, L** (2009): On the Young's modulus of a auxetic composite structure. *Mechanics Research Communications*, 36: 294–301.
- Geraets, W.G.M.** (1998): Comparison of two methods for measuring orientation. *Bone* 23: 383–388.
- Geraets, W.G.M.; Van der Stelt, P.F.; Lips, P., Elders, P.J.M.; Van Ginkel, F.C.; Burger, E.H.** (1997): Orientation of the trabecular pattern of the distal radius around the menopause. *Journal of Biomechanics* 30: 363–370.
- Geraets, W.G.M.; Van Ruijven, L.J.; Verheij, J.G.C.; Van der Stelt, P.F.; Van Eijden, T.M.G.J.** (2008): Spatial orientation in bone samples and Young's modulus. *Journal of Biomechanics* 41: 2206–2210.

- Geraets, W.G.M., Van der Stelt, P.F., Lips, P., van Ginkel, F.C.**(1998): The radiographic trabecular pattern of hips in patients with hip fractures and in elderly control subjects. *Bone* 22: 165–173.
- Geraets, W.G.M.; Van Ruijven, L.J.; Verheij, J.G.C.; Van Eijden, T.M.G.J.; Van der Stelt, P.F.** (2006): A sensitive method for measuring spatial orientation in bone structures. *Dentomaxillofacial Radiology* 35: 319–325.
- Giesen, E.B.W.; Van Eijden, T.M.G.J.** (2000): The three-dimensional cancellous bone architecture of the human mandibular condyle. *Journal of Dental Research* 79, 957–963.
- Gomberg, B.R.; Saha, P.K.; Wehrli, F.W.** (2003): Topology-based orientation analysis of trabecular bone networks. *Medical Physics* 30: 1–11.
- Harrigan, T.P.; Mann, R.W.** (1984): Characterization of microstructural anisotropy in orthotropic materials using a second rank tensor. *Journal of Materials Science* 19: 761–767.
- Hoffmeister, B.K.; Smith, S.R.; Handley, S.M.; Rho, J.Y.** (2000): Anisotropy of Young's modulus of human tibial cortical bone. *Medical and Biological Engineering and Computing* 38: 333–338.
- Homminga, J.; Van-Rietbergen, B.; Lochmu" ller, E.M.; Weinans, H.; Eckstein, F.; Huiskes, R.** (2004): The osteoporotic vertebral structure is well adapted to the loads of daily life but not to infrequent "error" loads. *Bone* 34: 510–516.
- Hou, F.J.; Lang, S.M.; Hoshaw, S.J.; Reimann, D.A.; Fyhrie, D.P.** (1998): Human vertebral body apparent and hard tissue stiffness. *Journal of Biomechanics* 31: 1009–1015.
- Huiskes, R.** (2000): If bone is the answer, then what is the question? *Journal of Anatomy* 197: 145–156.
- Jankowski, A.F.; Tsakalacos, T.** (1985): The effect of strain on the elastic constants of noble metals. *J. Phys. F: Met. Phys.* 15: 1279–1292.
- Jankowski, A.F.** (1988): Modelling the supermodulus effect in metallic multilayers. *J. Phys. F: Met. Phys.*, 18: 413–427
- Kabel, J.; van Rietbergen, B.; Dalstra, M.; Odgaard, A.; Huiskes, R.** (1999): The role of an effective isotropic tissue modulus in the elastic properties of cancellous bone. *Journal of Biomechanics* 32: 673–680.
- Katz, J.L.; Meunier, A.** (1987): The elastic anisotropy of bones. *Journal of Biomechanics* 20(11/12): 1063–1070
- Keaveny, T.M.; Morgan, E.F.; Niebur, G.L.; Yeh, O.C.** (2001): Biomechanics of trabecular bone. *Annual Reviews of Biomedical Engineering* 3: 307–333.

- Lakes, R.S.; Katz, J.L.; Sternstein, S.S.** (1975): Torsional and biaxial dynamic and stress relaxation properties of bovine and human cortical bone. *ASME Biomechanics Symposium* (eds, Skalak, R. and Nevern, R.M.) 10, 133–134. American Society of Mechanical Engineers, New York.
- Lakes, R.S.; Katz, J.L.** (1979a): Viscoelastic properties and behavior of cortical bone: part II: Relaxation mechanisms. *Journal of Biomechanics* 12: 679–687.
- Lakes, R.S.; Katz, J.L.** (1979b): Viscoelastic properties and behavior of cortical bone: part III: A non-linear constitutive equation. *Journal of Biomechanics* 12: 689–698.
- Lang, S.B.** (1969): Elastic coefficients of animal bone. *Science* 165: 287–288.
- Lang, S.B.** (1970): Ultrasonic method for measuring elastic coefficients of bone and the results on fresh and dried bovine bones. *IEEE Trans. Bio-Med. Engng.* 17: 101–105.
- Munteanu, L.; Chiroiu, C.; Chiroiu, V.** (2002) : Nonlinear dynamics of the left ventricle. *Physiological Measurement*, Institute of Physics Publ., 23: 417–435.
- Munteanu, L.; Donescu, St.; Chiroiu, V.** (2006): An inverse problem for the motion of blood in small vessels. *Physiological Measurement*, Institute of Physics Publishing, 27: 865–880.
- Odgaard, A.** (1997): Three-dimensional methods for quantification of cancellous bone architecture. *Bone* 20: 315–328.
- Pidaparti, R.M.V.; Turner, C.H.** (1997): Cancellous bone architecture: advantages of nonorthogonal trabecular alignment under multidirectional joint loading. *Journal of Biomechanics* 30: 979–983.
- Popescu, H.; Chiroiu, V.** (1981): *Optimum design of structures* (in Romanian), Publishing House of the Romanian Academy.
- Saltikov, S.A.** (1958): *Stereometric Metallography*, second ed. Metallurgizdat, Moscow.
- Singh, I.** (1978): The architecture of cancellous bone. *Journal of Anatomy* 127: 305–310.
- Snyder, B.D.; Piazza, S.; Edwards, W.T.; Hayes, W.C.** (1993): Role of trabecular morphology in the etiology of age-related vertebral fractures. *Calcified Tissue International* 53 (Suppl. 1): s14–s22.
- Teodosiu, C.** (1982): *Elastic models of crystal defects*. Publishing House of the Romanian Academy, Springer-Verlag.
- Turner, C.H.** (1992): On Wolff's law of trabecular architecture. *Journal of Biomechanics* 25: 1–9.

Van Eijden, T.M.G.J.; Van der Helm, P.N.; Van Ruijven, L.J.; Mulder, L. (2006): Structural and mechanical properties of mandibular condylar bone. *Journal of Dental Research* 85: 33–37.

Van Lenthe, G.H.; Huiskes, R. (2002): How morphology predicts mechanical properties of trabecular structures depends on intraspecimen trabecular thickness variations. *Journal of Biomechanics* 35: 1191–1197.

Van Rietbergen, B.; Weinans, H.; Huiskes, R.; Odgaard, A. (1995): A new method to determine trabecular bone elastic properties and loading using micromechanical finite-element models. *Journal of Biomechanics* 28: 69–81.

Van Ruijven, L.J.; Giesen, E.B.W.; Van Eijden, T.M.G.J. (2002): Mechanical significance of the trabecular microstructure of the human mandibular condyle. *Journal of Dental Research* 81(10): 701–710.

Van Ruijven, L.J.; Giesen, E.B.W.; Farella, M.; Van Eijden, T.M.G.J. (2003): Prediction of mechanical properties of the cancellous bone of the mandibular condyle. *Journal of Dental Research* 82(10): 819–823.

Veenland, J.F.; Link, T.M.; Konermann, W.; Meier, N.; Grashuis, J.L.; Gelsema, E.S. (1997): Unraveling the role of structure and density in determining vertebral bone strength. *Calcified Tissue International* 61: 474–479.

Whitehouse, W.J. (1974): The quantitative morphology of anisotropic trabecular bone. *Journal of Microscopy* 101: 153–168.

Wolff, J. (1892): *Das Gesetz der Transformation der Knochen*. Berlin: A. Hirschwald. Translated as *The Law of Bone Remodeling* (eds. Maquet P. and Furlong, R.). Berlin: Springer (1986).

Zysset, P. (1994): *A constitutive law for trabecular bone*. PhD thesis École Polytechnique Fédérale de Lausanne.

